Journal of Macromolecular Science, Part A
Publication details, including instructions for authors and subscription information:
http://www.informaworld.com/smpp/title~content=t713597274

Free Radical Scavenging Magnetic Iron-Based Nanoparticles in Hyperbranched and Linear Polymer Matrices

Gitanjal Deka[a]; Harekrishna Deka[a]; Niranjan Karak[a]
[a] Advanced Polymer and Nanomaterial Laboratory, Department of Chemical Sciences, Tezpur University, Tezpur, Assam, India

To cite this Article Deka, Gitanjal , Deka, Harekrishna and Karak, Niranjan(2009) 'Free Radical Scavenging Magnetic Iron-Based Nanoparticles in Hyperbranched and Linear Polymer Matrices', Journal of Macromolecular Science, Part A, 46: 11, 1128 — 1135
To link to this Article: DOI: 10.1080/10601320903245474
URL: http://dx.doi.org/10.1080/10601320903245474

Journal of Macromolecular Science®, Part A: Pure and Applied Chemistry (2009) **46**, 1128–1135

ISSN: 1060-1325 print / 1520-5738 online
DOI: 10.1080/10601320903245474

Taylor & Francis
Taylor & Francis Group

Free Radical Scavenging Magnetic Iron-Based Nanoparticles in Hyperbranched and Linear Polymer Matrices

GITANJAL DEKA, HAREKRISHNA DEKA and NIRANJAN KARAK*

Advanced Polymer and Nanomaterial Laboratory, Department of Chemical Sciences, Tezpur University, Tezpur-784028, Assam, India

Received May 2009, Accepted June 2009

Magnetic iron nanoparticles are attracting a great deal of research and application interest in diversified fields. In this present investigation, iron nanoparticles were prepared by a *in-situ* chemical reduction technique in a combination of polyaniline (PANI)-polyacrylamide (PA) and PANI-hyperbranched polyurethane (HBPU) matrices to judge the suitability of hyperbranched system. The formation of the nanoparticles in polymer matrices has been investigated by FTIR, UV, XRD, SEM and TEM studies. Narrower size with better dispersion and more stable nanoparticles were found in a hyperbranched matrix system compared to a linear one. The particle size was found to be in the range of 10–20 nm and 12–35 nm in HBPU-PANI and PA-PANI matrices, respectively. Both the nanocomposites exhibit synergistic free radical scavenging capability towards 2,2-diphenyl-1-picrylhydrazyl (DPPH). The magnetic hysteresis loop of the nanocomposites indicates the super-paramagnetic behavior. The hyperbranched system is more thermostable than the linear system by 70°C.

Keywords: Magnetic iron-based nanoparticles, free radical scavenging, hyperbranched polyurethane, thermal property, magnetic property

1 Introduction

The expanding horizon of nanotechnology has been leading to the genesis of a multitude of novel utilities (1–2). In recent years, the myriad synthesis routes, modulation of surface features and application-based exploitation of nanoparticles have instigated tremendous prospective. Materials with both electric and magnetic properties are very interesting in research as well as the application field. Iron is one of the most widely used noble metals that find their applications in its colloidal or nanocrystalline form. The iron based nanoparticles has attracted much attention (3) because of their potential applications in many industrial and biological fields, such as mineral separation (4), heat transfer applications (5), electro-photography (6), radical scavenging capacity (7). But the foremost challenge of the nanocrystalline super-paramagnetic metals is to protect them from rapid environmental degradation.

In this context, nanoparticles in polymer matrices have recently emerged as an active field of research (8–10). This is due to their (a) enhanced stability, (b) difference in physical and chemical properties, (c) film forming ability of the polymer, etc. In the domain of polymer matrix, polyacrylamide (PA) is being widely used as a water soluble polymer for their physical and biological activity (11). Recently, the use of hyperbranched polymer in the field of nanocomposites have gaining considerable attention as they have better control over size, shape and structure of metal-nanoparticles than that of linear polymers (12). Hyperbranched polyurethane (HBPU) is one such category providing more stabilization of the nanodomain via interactions with their various types of groups present (13). Another important feature of HBPU is its tailor made properties.

Again, a great deal of interest is being paid in the studies of polyaniline (PANI)/iron based nanocomposites, because they possess excellent electric and magnetic properties which inclined them towards the applications in battery, microwave absorbing material, etc. (14). But it is difficult to prepare homogeneous and stable PANI/nanoparticle composites by conventional method as PANI is not easy to molten in nature and generally insoluble in common solvents (15). Owing to aforesaid intricacy, an *in-situ* chemical oxidative polymerization approach is adopted to synthesize PANI/iron based nanocomposites in presence of different matrices.

*Address correspondence to: Niranjan Karak, Advanced Polymer and Nanomaterial Laboratory, Department of Chemical Sciences, Tezpur University, Tezpur-784028, Assam, India. Tel: +91 3712 267209 (5086); Fax: +91 3712 267007; E-mail: karakniranjan@yahoo.com

Furthermore, it's worthwhile to note that the oxidizability and the antioxidant properties of polymer nanocomposite and polyphenolic compounds as found in a number of food items bear considerable similarity (16). The antioxidant characteristic of a molecule is commonly tested using 2,2-diphenyl-1-picrylhydrazyl (DPPH) in methanol.

Herein, authors wish to report the preparation and characterization of iron nanoparticles in PA-PANI and HBPU-PANI matrices. The free radical scavenging capacity of the iron nanocomposites was investigated against DPPH. The thermal stability and magnetic properties of the iron nanoparticles in the above systems have also been studied. A comparison has been drawn out on the properties of the HBPU and PA matrices for the studied nanocomposites.

2 Experimental

2.1 Materials

Acrylamide (SD Fine Chemical Ltd., Mumbai), lead mono-oxide (SD Fine Chemical Ltd., Mumbai), potassium persulphate (Merck, India), anhydrous iron (III) chloride (Merck, India), sodium borohydride (Merck, India), HCl (Merck, India), 2,4-toluene diisocyanate (TDI, Sigma Aldrich), methanol (Merck, India) were used as received. Glycerol (Merck, India) and poly(ε -caprolactone) diol (PCL, Solvay Co., M_n = 3000 g/mol) were used after drying in an oven. Aniline (Merck, India) was vacuum distilled prior to used and kept in a dark place. N,N-dimethylformamide (DMF, Merck, India) was dried over CaO, vacuum distilled and kept in 4A type molecular sieves before use. Monoglyceride of the *Mesua ferrea* L. seed oil was prepared by the standard glycerolysis procedure. 2,2-Diphenyl-1-picrylhydrazyl (DPPH, HIMEDIA) (Molecular weight = 394.33 g/mol) was used for the free-radical scavenging test. Other reagents are of reagent grade and used without further purification.

2.2 Preparation of Polymer Matrix

In a three-necked round bottom flask, 2 g of acrylamide was dissolved in 15 mL of water. 0.02 g (1%) of potassium persulphate was added as initiator into the solution. It was then heated to (70 ± 2)°C for half an hour with constant stirring to get polyacrylamide.

2.3 Preparation of Hyperbranched Polymer

The hyperbranched polyurethane was prepared by pre-polymerization technique. At first, a pre-polymer was prepared from 2 mol of poly(ε-caprolactone) diol, 3 mol of monoglyceride of *Mesua ferrea* L. seed oil and 7.5 mol of TDI and a polymer was obtained finally by the reaction of the pre-polymer with glycerol of 2.5 mol in DMF as a solution of 25–30% solid content (w/v).

2.4 Preparation of Iron Nanoparticles

In the prepared polyacrylamide solution, a weighed amount (0.5 wt% with respect to PA) of $FeCl_3$ solution was mixed. 1 mL of distilled aniline was dissolved in 4 mL water in the presence of dilute HCl and the solution was added dropwise in the above mixture. The color of the mixture turns black from yellow within 10 min. The UV spectrum of this solution was taken immediately to confirm the formation of nanoparticles. This black solution was then cast to thin film and dried under ambient conditions for further analysis. The above method was also employed to prepare the iron nanoparticles in HBPU matrix using HBPU instead of PA.

2.5 Measurements

UV spectra of the samples were recorded in a Shimadzu (UV-2550, USA) UV spectrophotometer by using 0.001% solution in water for water soluble samples and in DMF for the water insoluble samples. X-ray diffraction (XRD) study was carried out at room temperature (ca. 27°C) by a Rigaku X-ray diffractometer (Miniflex, UK) at scanning rate of 5°/min over the range of 2θ = 10–90°. FTIR spectra of the compounds were taken by Nicolet (Impact 410, Madison) FTIR spectrophotometer by using KBr pellets. The size and distribution of iron nanoparticles were studied by JEOL JEMCXII, transmission electron microscopes (TEM) at operating voltage 80 kV. The surface morphology of the nanocomposites was done by scanning electron microscope, JEOL JSM-6390LV. The surface of the samples was platinum coated before testing for this purpose. The thermal analysis was done by a Shimadzu, USA thermal analyzer, TG 50, at 5°C/min heating rate under the nitrogen flow rate of 30 mL/min. Magnetic properties were studied by vibrating sample magnetometer (Lakeshore 7410) within the range +20,000 G to −20,000 G at room temperature.

For the free radical scavenging analysis, DPPH was dissolved in methanol to make 8×10^{-5} M solution. In a 3 mL quartz cuvette, 2.5 mL of DPPH solution and 100 mL of the test sample were combined and settled in the holder. Absorbance at 517 nm due to DPPH radical species was monitored after an incubation period of 30 min in the dark at room temperature. Analysis was carried out in triplicates and percent scavenging was calculated as:

$$\%\,\text{scavenging} = 100\times(1-A_{\text{DPPH after reacting with the test sample}}/A_{\text{free DPPH}}) \quad (1)$$

3 Results and Discussions

3.1 Preparation of Iron Nanoparticles

The iron nanoparticles were formed by *in-situ* reduction of ferric chloride in the matrix of PA and HBPU systems by aniline. In this process, Fe^{3+} ions are reduced to Fe^0

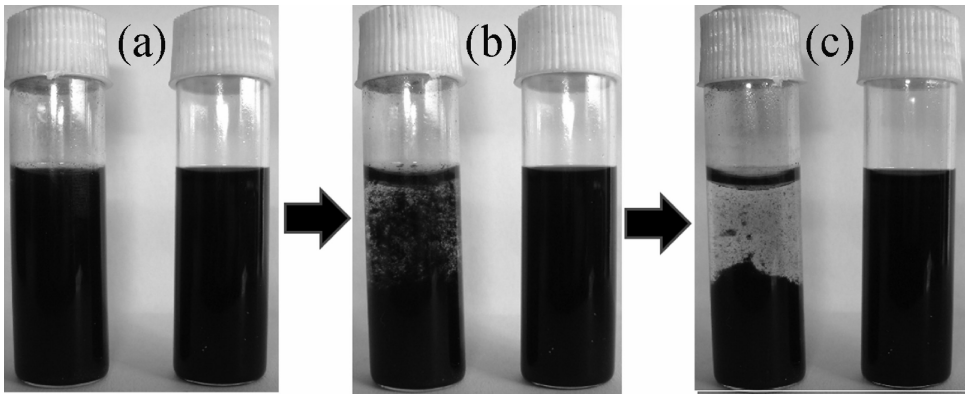

Fig. 1. A pictorial presentation showing stability the nanocomposites (a) After 2 h, (b) After 1 month and (c) After 3 month.

while aniline simultaneously gets polymerized to polyaniline in the solution of polyacrylamide and hyperbranched polyurethane. Thus, there is no need of any external reducing agent, which partly follows the principle of green chemistry. Nanoparticles have very high surface to volume ratio and hence, very high surface energy, therefore have a great tendency to agglomerate (17). Polymers are being used as a stabilizer for these nanoparticles in a chemical synthesis route of metal colloids, since they have the ability to prevent agglomeration and precipitation of the nanoparticles. The synthesis of polymer nanocomposites is also advantageous from the viewpoint of ease of processing and fabrication which helps their use in various fields. In the present study, the metal salt was dispersed in the pre-polymer solution, which has low viscosity and hence, the particles are well-dispersed. Further, the amide groups of the polyacrylamide and the large numbers of active surface hydroxyl groups of hyperbranched polyurethane along with the urethane groups form stable complexes with the metal ions (Fe^{3+}). These phenomena help in uniform dispersion and better stability compared to non-polymeric system. However, even though the macromolecular chains of polyacrylamide protect the surface of the Fe^0 nanoparticles from being agglomerated and also reduce the oxidation of the metal nanoparticles by the oxygen in air and water after reduction, but the stability of iron nanoparticles in hyperbranched polyurethane was found to be greater. A pictorial presentation describing better stability in the HBPU-PANI matrix compared to PA-PANI is given in Figure 1. This better stability is due to the fact that the presence of urethane groups, ester linkages, surface hydroxyl groups in hyperbranched polyurethane facilitates the formation of complex of Fe^{3+} ions with polymer chain and thus gives homogeneous dispersion of nanoparticles in the matrix and the unique structural architecture of hyperbranched polymer restricts the mobility of the nanoparticles after formation (18). Thus, the present stable iron/iron oxide decorated nanocomposite has the film forming ability along with other useful properties.

3.2 Characterization of Iron Based Nanoparticles

XRD technique is usually used to acquire information about the crystallinity of the nanoparticles and the polymer. The XRD pattern of the polymer matrices and their nanocomposite with iron nanoparticles were shown in the Figure 2. The amorphous nature of the nanoparticles and their nanocomposites can be observed by the absence of any distinct diffraction pattern corresponding to iron/iron-oxide (19, 20) in the case of hyperbranched polymer (Fig. 2(d)). This can be attributed to the formation of well dispersed and very small particles of iron/iron oxide in hyperbranched matrix. In Figure 2 (e), the XRD pattern of the pure HBPU-PANI shows sharp peaks at $2\theta = 21.2^\circ$ (4.19 A°) and 23.4° (3.81 A°) are due to crystallinity of poly(ε -caprolactone) diol (PCL) moiety (21). Whereas, the XRD

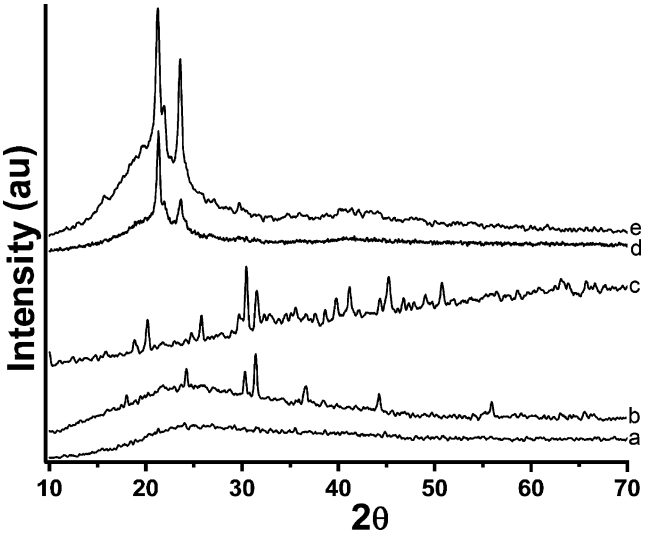

Fig. 2. XRD pattern of the polymer matrix and corresponding nanocomposite (a) PA-PANI pure polymer system, (b) iron-PA-PANI nanocomposite, (c) iron-HBPU-PANI nanocomposite system annealed at 600°C for 5 h, (d) pure-HBPU and (e) iron-HBPU-PANI nanocomposite system.

pattern of the iron/iron-oxide HBPU-PANI nanocomposite doesn't show any distinct peak besides the peaks present in pure HBPU (Fig 2. (d)). Peaks in this case shifted slightly towards a higher angle with a decrease of intensity from its position in pure polymer due to its interaction with nanoparticles. The XRD pattern of this nanocomposite after annealed at 600°C for 5 h (19) was also observed in Figure 2 (c). The pattern is dominated by the strong and sharp peaks of different crystallographic phases of iron oxides, due to the burning out of the matrix polymer and an increase in size of the nanoparticles during oxidation. The peak at the $2\theta = 44.5^{\circ}$ indicates the presence of the zero-valent iron and the other peaks are due to the presence of iron oxides. This is due to the partial transformation of Fe^0 to Fe^{2+} or Fe^{3+} (iron oxide) state during annealing under open atmosphere (22). Well defined diffraction peaks of different phases of iron and iron-oxide nanoparticles were observed in the linear nanocomposites without annealing (Fig. 2 (b)) (23), whereas the pure polymer matrices does not show any sharp peak indicating their amorphous character. As the TEM images (discussed later) reveals, the particles embedded in linear matrix are of large in size, their crystallinity can be well observed in the diffractogram.

Metal nanoparticles, with a much finer dimension, exhibits absorption bands or a broad region of absorption in the ultraviolet-visible range. These bands are due to the excitation of plasmon resonance or inter band transition. So each metal nanoparticle has their characteristic absorption band at a particular wavelength. Thus, UV-visible absorption spectra were employed to characterize the iron nanoparticles embedded in polymer matrix. The iron nanoparticles dispersed in all the polymer matrices show maximum absorption at around 320–340 nm which is characteristic of iron/iron-oxide nanoparticle surface plasmon resonance (Figure 3). While their respective polymer matrices do not show any bands in the aforesaid region. The plasmon absorption peak shifts to a higher wavelength with the increase of aggregation of the nanoparticles (24). Furthermore, an attempt was made to observe the stability of the PA-PANI and HBPU-PANI nanocomposites with the help of a UV spectrophotometer. Absorbance of the nanocomposites was taken after 24 h and one month. A red shift, with respect to time, was observed from 310 to 345 nm for an iron-PA-PANI system, while this shift is only 10 nm for iron-HBPU-PANI nanocomposites (Fig. 3). Thus, the UV study also predicts better stability in the HBPU matrix. It is well known that iron nanoparticles are easily oxidized by air and water (22). This red shift may be due to the increase in size by the modification of the surface of the iron nanoparticles to iron oxides (core shell iron nanoparticle) (25). This was clearly observed in the TEM images (discussed later).

FTIR analysis was performed to characterize the interactions of the resulting iron-based nanoparticles with the matrices, as depicted in Figure 4. The regions in the FTIR spectra for iron/iron oxide in different matrices were

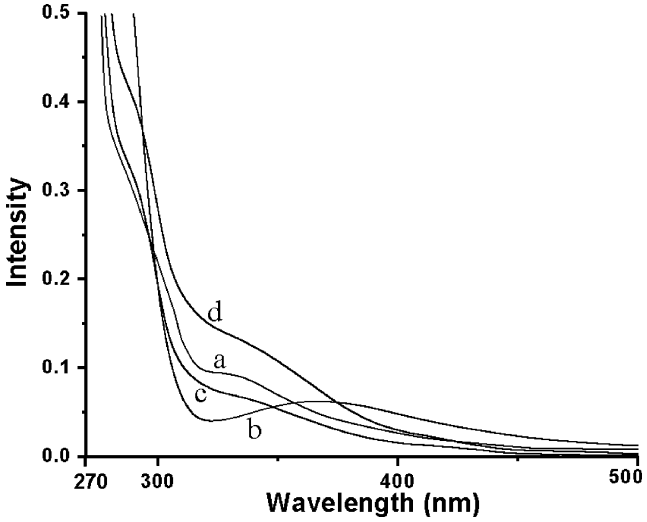

Fig. 3. UV spectra of (a) iron-PA-PANI nanocomposite after half an hour, (b) iron-PA-PANI nanocomposite after 24 h, (c) iron-HBPU-PANI nanocomposites after half an hour and (d) iron-HBPU-PANI nanocomposites after 24 h.

compared. The FTIR band for Fe-oxide appears within 590–550 cm^{-1}, correspond to the vibration of Fe—O bonds in the tetrahedral sites and in the octahedral sites (26). After annealing, the nanocomposites lost most of the IR bands other than the band at 2370, 1630, 1160 and 565 cm^{-1} band which is attributed to the formation of oxides of iron with carbonaceous coating (27). The IR band at 1650–1670 cm^{-1} is due to the overlapping of >C=O stretching, $-NH_2$ bending and coupling modes between C—N stretching and >N—H bending. It is also due to the interaction between amide group or urethane group and iron-based

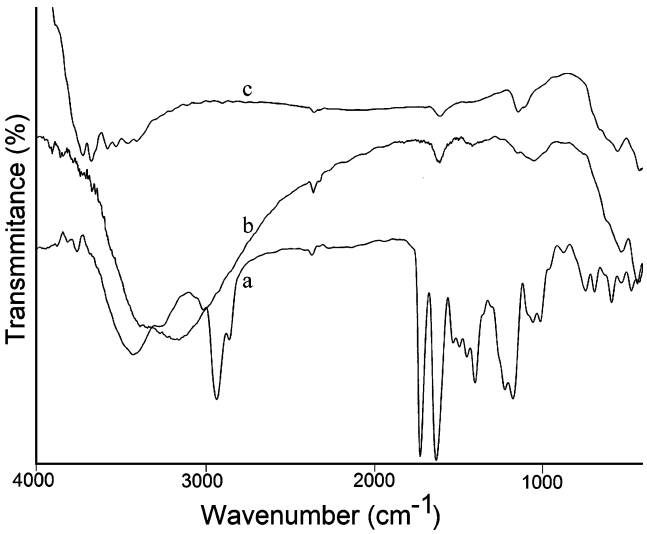

Fig. 4. FTIR spectra of (a) iron-HBPU-PANI nanocomposite, (b) iron-PA-PANI nanocomposite and, (c) iron-HBPU-PANI nanocomposite system annealed at 600°C for 5 h.

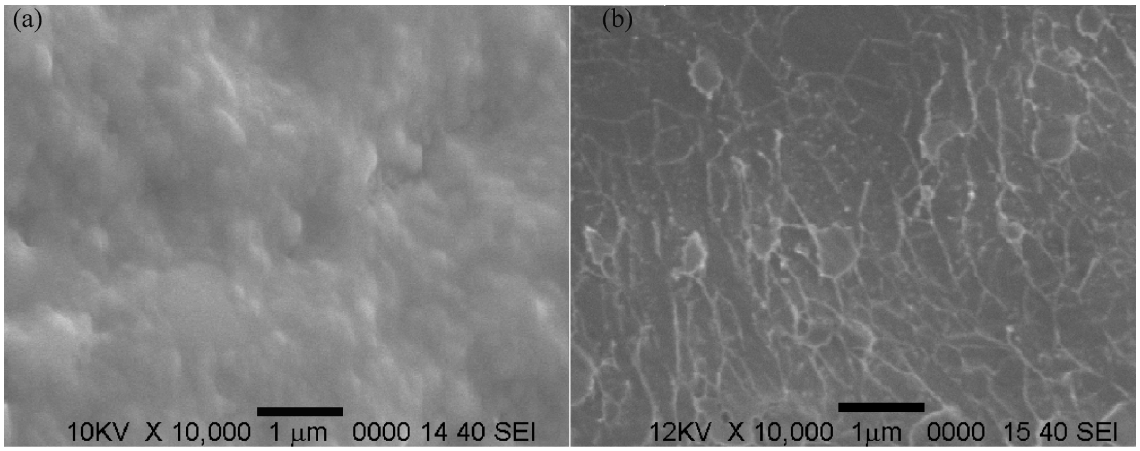

Fig. 5. SEM images of the iron-based nanocomposite (a) HBPU-PANI matrix and (b) PA-PANI matrix.

nanoparticles. The characteristic IR bands for the presence of PANI in the nanocomposites are found at 1450 cm^{-1} (N=C_{ar}=N) and 1100 cm^{-1} (C–N). Upon comparison of the IR spectra, it can be observed that the intensity of the above bands decreases or disappears after annealing, due to the burning of the polymer phase. In the case of the Fe/HBPU system, the changes occur in the region of 2900 cm^{-1}. The $-CH_2$ symmetric and asymmetric stretching bands were observed at 2800 cm^{-1} and 2900 cm^{-1}, respectively.

The surface morphology of the polymer iron nanocomposites were characterized by SEM micrographs. The SEM image of the iron-HBPU-PANI nanocomposite shows very few nanoparticles on the surface conforming to the fact that the nanoparticles tend to disperse towards the bulk of the polymer matrix (Fig. 5). Again, the SEM image of iron-PA-PANI nanocomposite indicates a very interesting observation that polyaniline having nanofibrous morphology in its early age (28) gets dispersed and protected in the polyacrylamide matrix along with the iron nanoparticles. This observation may lead to other avenues to utilize this product in the field of conducting polymer nanofiber.

The morphology, size and size distribution of the iron nanoparticles were depicted in the TEM micrograph (Fig. 6). The spherical and homogenously dispersed iron nanoparticles with an average particle size of diameter 10 nm within a size window of (5–15) nm can be visualized in a HBPU-PANI matrix of TEM image. While in PA-PANI matrix, the nano particles are distributed within a size window of (20–30) nm. The histograms for the particle size distribution clearly indicate that the size distribution of the nanoparticles is narrower in the HBPU matrix than the linear one (Fig. 7).

In the TEM analysis, it is observed that the iron nanoparticles are coated with a thin oxide layer of 3 to 5 nm (Fig. 6). So the nanoparticles are of surface modified core shell type (29). Interestingly, it was observed that the dispersion of the nanoparticles was better in HBPU than linear one and unlike linear matrix no observable oxide layer was formed over the nanoparticles in hyperbranched matrix. Thus, it

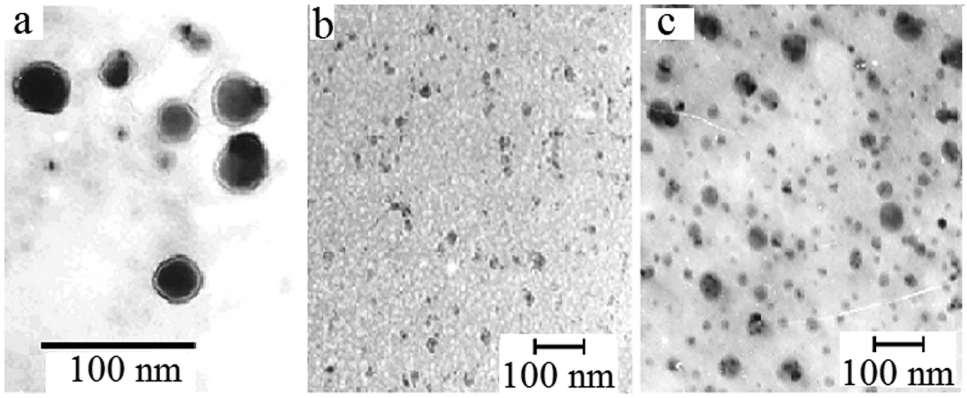

Fig. 6. TEM micrograph of the iron-based nanocomposite (a) PA-PANI system at high resolution showing the oxide layer over the iron nanoparticles, (b)HBPU-PANI system and (c) PA-PANI system.

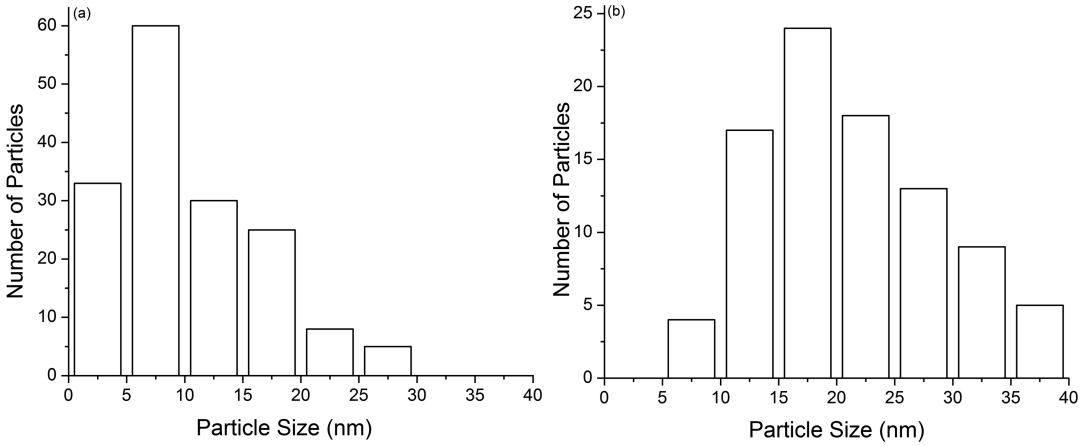

Fig. 7. Histogram for size distribution of (a) iron-HBPU-PANI nanocomposite and (b) iron-PA-PANI nanocomposite.

can be explained that hyperbranched polyurethane provides enhanced dispersibility and stability of the nanoparticles due to the unique architectural feature of channel and cavity in the HBPU (13). These structural features generate a confined structural geometry and thereby stabilize the nanoparticles. The better distribution is due the presence of large numbers of polar functionalities in the hyperbranched matrix compared to the linear polyacrylamide matrix.

3.3 Free Radical Scavenging Activity

It's interesting to note that iron-PA-PANI nanocomposite has the best DPPH free radical scavenging (30) ability compared to the other systems, about 84%, whereas the pure PA-PANI matrix has only 30% scavenging. Figure 8 compares the % radical scavenging by different nanocomposite systems. There pure HBPU shows 45% radical scavenging and the iron-HBPU-PANI nanocomposite shows about 67% scavenging. The radical scavenging capability of the HBPU matrix can be attributed to the scavenging ability of the urethane group present in the HBPU matrix, and this property get improved by the incorporation of the iron nanoparticles. The better scavenging property of linear composite system than the hyperbranched one can be attributed to the presents of more surface exposed nanoparticles in the linear composite system (from SEM images, Fig. 5). But in the case of the hyperbranched composite system, the nanoparticles are most likely to be towards the bulk of the matrix because of the unique structural feature of hyperbranched polymers, which stops the surface activity of the iron nanoparticles.

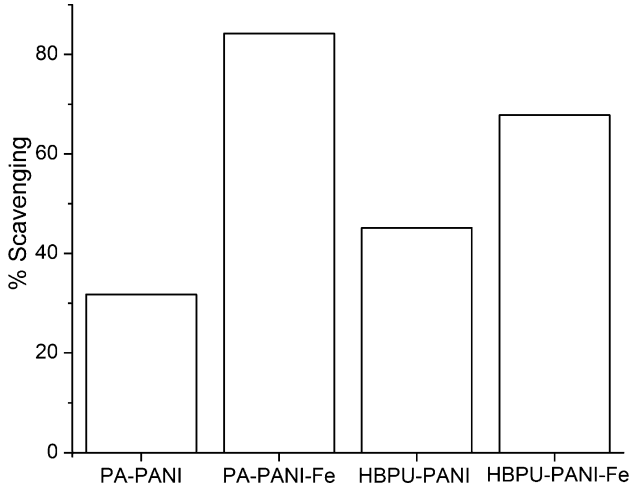

Fig. 8. % scavenging of different systems.

3.4 Magnetic Behavior

The ferromagnetic behavior of the polymer iron nanocomposites are demonstrated by the hysteresis loop measurement using a vibrating sample magnetometer. Figure 9 shows the magnetization curve of the nanocomposites at room temperature. From the figure, it is clear that the magnetization of the nanocomposites did not reach the saturation value even at the maximum applicable magnetic field of the instrument. However, it is obvious that the magnetic particles present in the polymer matrix were of single domain super-paramagnetic in nature due to the very small size of the iron nanoparticles which can be explained by very low coercivity and retentivity of the hysteresis loop (31) (Fig. 9). But the polymer being diamagnetic in nature, supporting the iron nanoparticles decreases the magnetic nature of the nanocomposites to a very effective extent, and it is further decreased by the non-magnetic phase of the oxide layer formed over the iron nanoparticles (31, 32). The magnetization curve of the hyperbranched composite system has lower coercivity and retentivity than the linear one and is due to much smaller sized nanoparticles in the

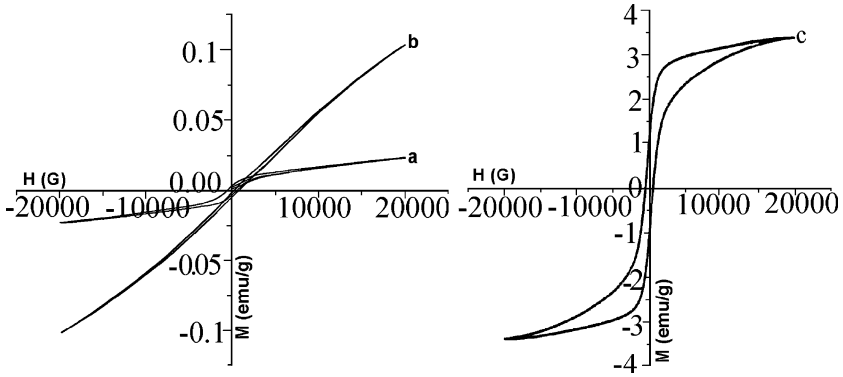

Fig. 9. A representative magnetization curve of nanocomposites (a) hyperbranched matrix, (b) linear matrix and (c) annealed iron-HBPU-PANI nanocomposite, at room temperature.

hyperbranched system. The magnetization value at a particular applied field is also greater in the hyperbranched system due to the formation of a larger number of particles than the linear one. The retentivity values (as seen in Fig. 8) are 0.0005 emu/g and 0.000187 emu/g for iron-HBPU-PANI nanocomposite and iron-PA-PANI nanocomposite, whereas the coercivity values are 90 G and 220 G, respectively.

Figure 9 also depicts the hysteresis loop of the annealed sample. The loop width in this case slightly broadens due to the increase in size of the nanoparticles by the oxidation during annealing in air, which results in the increase of the coercivity (19, 31). Also, the saturation magnetization increased here due to the burning of the polymer leaving a carbon-complexed coating. The retentivity and coercivity value for the annealed sample, as seen in Figure 9, are 1.02 emu/g and 470 G, respectively.

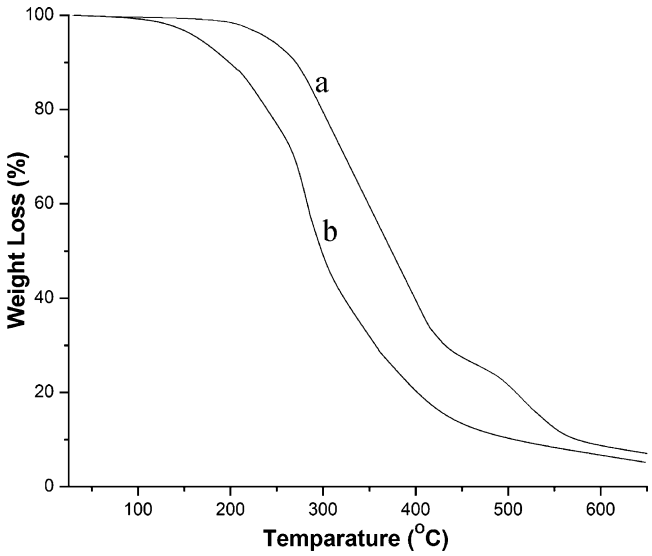

Fig. 10. TGA curves of (a) iron-HBPU-PANI nanocomposite and (b) iron-PA-PANI nanocomposite.

3.5 Thermal Property

The relative thermal stability of the iron nanocomposites is investigated by TGA. A two step degradation pattern (Fig. 10) with enhanced thermal stability of the iron-HBPU-PANI and then the iron-PA-PANI nanocomposites is observed. The characteristic thermal degradation temperatures are reported in Table 1. 70°C, 65°C and 58°C shifts of the first initial decomposition temperature and temperature corresponding maximum rate of weight loss for the first step and second initial decomposition temperature were observed for iron-HBPU-PANI nanocomposites with respect to the iron-PA-PANI nanocomposite, respectively. This is due to the restricted motion of the hyperbranched polymer chains (18). It is also noticeable that not only initial decomposition temperature increases, but the weight residue is also higher for iron-HBPU-PANI than the iron-PA-PANI system.

Table 1. Thermal stability data of the nanocomposites

Code	T_{onset} (°C)	T_{max} (°C)	T_{end} (°C)	*Char Residue at 650°C*
iron-PA-PANI nanocomposite	142	290	490	7
iron-HBPU-PANI nanocomposite	212	355	548	13

4 Conclusions

Thus, the reported system highlights a simple and step forward process for the preparation of iron based nanoparticles. This simple reduction technique yields well dispersed iron nanoparticles in different polymer matrices. The dispersion is enhanced in the case of hyperbranched polyurethane with respect to polyacrylamide matrix. The sizes of iron nanoparticles were also smaller and more uniform within the HBPU-PANI system than the linear system. The nanocomposites exhibit observable free radical scavenging capability towards DPPH. The iron nanoparticles had super-paramagnetic behavior and the magnetization increases on annealing. From the observed results, it is expected to trigger application-oriented research in various other niches.

Acknowledgements

The authors express their gratitude and thanks to the research project assistance given by DST, India through the grant No. SR/S3/ME/13/2005-SERC-Engg, dated 9th April, 2007. Also, Mr. Gitanjal Deka thanks the Coordinator, Nanoscience and Technology, Department of Physics, Tezpur University. RSIC, NEHU, Shillong and CIF, IIT Guwahati are thankfully acknowledged for the TEM imaging and magnetometric analysis, respectively.

References

1. Teranishi, T., Hori, H. and Miyake, M. (1997) *J. Phys. Chem. B.*, 101, 5774–5776.
2. Volokitin, Y., Sinzing, J., de Jongh, L.J., Schmid, G., Vargaftik, M.N. and Moiseevi, I.I. (1998) *Nature.,* 384, 621–623.
3. Alivisatos, A.P. (1996) *Science.,* 271, 933–937.
4. Züm, C.Ü., Shahwan, T., Erôglu, A.E., Lieberwirth, I., Scott, T.B. and Hallam, K.R. (2008) *Chem. Eng. J.,* 144, 213–220.
5. Ponder, S., Darbab, J. and Mallouk, T. (2000) *Environ. Sci. Technol.*, 34, 2564–2569.
6. Sandhu, A. and Handa, H. (2005) *IEEE Trans. Magn.*, 41, 4123–4127.
7. Senyei, A., Widder, K., and Czerlinski, G. (1978) *J. Appl. Phys.*, 49, 3578–3583.
8. Jones, S.K., Winter, J.G., and Gray, B.N. (2002) *Int. J. Hyperthermia.*, 18, 117–128.
9. Kim, D.K., Zhang, Y., Voit, W., Rao, K.V., Kehr, J., Bjelke, B. and Muhammed, M. (2001) *Scripta Mater.*, 44, 1713–1717.
10. Tomalia, D.A. and Dvornic, P.R. (1994) *Nature.*, 372, 617–618.
11. Wang, C., Stewart, R.J. and Kopecek, J. (1999) *Nature.*, 397, 417–420.
12. Zhang, X. and Yan, D. (2008) *J. Phys. Chem. C.,* 112, 2330–2336.
13. Lu, H.W., Liu, S.H., Wang, X.L., Qian, X.F., Yin, J. and Zhu Z.K. (2003) *Mat. Chem. Phys.*, 81, 104–107.
14. Long,Y., Chen, Z., Duvail, J.L., Zhang, Z. and Wan, M. (2005) *Physica B.,* 370, 121–130.
15. Henglein, A. (1993) *J. Phys. Chem.*, 97, 5457–5471.
16. Marija, G.N., Jadranka, T.S., Bowmaker, G.A., Cooney, R.P., Thompson, C. and Kilmartin, P.A. (2004) *Curr. Appl. Phys.,* 4, 347–350.
17. Turkevich, J., Stevenson, P.C. and Hillier, J. (1951) *Discuss. Faraday Soc.*, 11, 55–75.
18. Karak, N. and Maiti, S. Dendrimers and Hyperbranched Polymers—Synthesis to Applications. MD publication Pvt. Ltd., New Delhi, 2008.
19. Li, Q., Li, H., Pol, V.G., Bruckental, I., Koltypin, Y., Calderon-Moreno, J., Nowik, I. and Gedanken, A. (2003) *New J. Chem.*, 27, 1194–1199.
20. Oh, S.J., Choi, C.J., Kwon, S.J., Jin, S.H., Kim, B.K. and Park, J.S. (2004) *J. Magnet. Magnet. Mater.*, 280, 147–157.
21. Karak, N., Rana, S. and Cho, J.W. (2009) *J. Appl. Polym. Sci.*, 112, 736–743.
22. Guo, L., Huang, Q., Li, X.Y. and Yang, S. (2001) *Phys. Chem. Chem. Phys.*, 3, 1661–1665.
23. Sun, Y.P., Li, X.Q., Cao, J., Zhang, W.X. and Pang, H.P. (2006) *Adv. Colloid. Interfac.*, 120, 47–56.
24. Dha, H.G., Kim, Y.H., Kim, C.W., Kwon, H.W. and Kang, Y.S. (2007) *Curr. Appl. Phys.*, 7, 400–403.
25. Kim, C.Y., Jang, S.C. and Yi, S.C. (2004) *J. Ceramic Processing Research.,* 5, 264–268.
26. Barrodo, E., Prieto, F., Medina, J. and Lopez, F.A. (2002) *J. Alloys. Compd.*, 335, 203–209.
27. Predoi, D. (2007) *Digest J. Nanomaterials and Biostructures.,* 2, 169–173.
28. Huang, J. (2006) *Pure. Appl. Chem.*, 78, 15–27.
29. Li, X.Q. and Zhang, W.X. (2006) *Langmuir.,* 22, 4638–4642.
30. Molyneux, P. (2004) *Songklanakarin. J. Sci. Technol.*, 26, 211–219.
31. Cha, H.G., Kim, Y.H., Kim, C.W. and Kang, Y.S. (2007) *Sensor Actuator B.,* 126, 221–225.
32. Wilson, J.L., Poddar, P., Frey, N.A., Srikanth, H., Mohomed, K., Harmon, J.P., Kotha, S. and Wachsmuth, J. (2004) *J. Appl. Phys.,* 95, 1439–1443.